Available online at www.sciencedirect.com

SciVerse ScienceDirect

Scripta Materialia 69 (2013) 53–56

Scripta MATERIALIA

www.elsevier.com/locate/scriptamat

Microbanding mechanism in an Fe–Mn–C high-Mn twinning-induced plasticity steel

I. Gutierrez-Urrutia* and D. Raabe

Max-Planck-Institut für Eisenforschung, Max-Planck Str. 1, D-40237 Düsseldorf, Germany

Received 12 February 2013; revised 10 March 2013; accepted 12 March 2013
Available online 19 March 2013

We study the microbanding mechanism in an Fe–22Mn–0.6C (wt.%) twinning-induced plasticity steel. Dislocation substructures were examined by electron channeling contrast imaging and electron backscatter diffraction. We observe a pronounced effect of the strain path on microbanding, which is explained in terms of Schmid's law. Microbands created under shear loading have a non-crystallographic character. This is attributed to the microbanding mechanism and its relation with the dislocation substructure. Further insights into the dislocation configuration of microbands are provided.

Keywords: Dislocation cell; Plastic deformation; Electron backscattering diffraction (EBSD); Electron channeling contrast imaging (ECCI); Austenitic steels

Recent investigations into the deformation structure in austenitic high-Mn steels, namely, Fe–Mn–C and Fe–Mn–Al–C alloys, have revealed a complex dislocation substructure formed by cells, cell blocks and Taylor lattices [1–6]. These dislocation configurations are formed at low deformation levels (true tensile strain <0.3) and are characterized by characteristic dislocation patterns. Cell blocks and Taylor lattices are delimited by geometrically necessary boundaries (GNBs), referred to as highly dense dislocation walls (HDDWs), and incidental dislocation boundaries (IDB), termed dislocation walls [7,8]. Cells are only defined by IDBs. The underlying mechanisms controlling the formation of dislocation structures are governed by specific dislocation reactions that are stress dependent [9]. Accordingly, dislocation patterning is strongly dependent on the crystallographic orientation [1,2,4]. The role of these dislocation substructures on the strain hardening behavior of high-Mn steels has been addressed recently [1,4]. Specifically, the combination of dislocation substructure hardening (at low and medium true tensile strains, <0.3) together with deformation twinning (at high true tensile strains, >0.3) leads to a multiple-stage strain hardening behavior resulting in permanent strain hardening up to high-deformation regimes and, hence, superior mechanical properties. In addition to these dislocation substructures, high-Mn steels can also develop microbands. These dislocation configurations have been reported in Fe–Mn–Al–C alloys deformed under tension [4,10–12]. Microbands are commonly characterized as paired dense dislocation layers which are separated from each other by a few hundred nanometers. They are associated with a strain localization phenomenon that is characterized by high local dislocation densities [13,14]. Unlike shear bands, which have a non-crystallographic alignment, microbands layers are often aligned with the {1 1 1} slip planes, i.e. they form crystallographic boundaries, and typically remain inside their respective host grains. Microbands may also contribute to the strain-hardening of high-Mn steels, although their specific kinetic role and hardening effects are still unclear [4,10,15]. Therefore, the present study aims at clarifying the microband formation mechanism in high-Mn steels. We have investigated the dislocation substructures, in particular those associated with microbands, obtained under different strain paths, namely, tension and shear, in an Fe–22Mn–0.6C (wt.%) high-Mn twinning-induced plasticity (TWIP) steel by combined electron channeling contrast imaging (ECCI) and electron backscatter diffraction (EBSD). The crystallographic orientation dependences of the dislocation patterns as well as of the dislocation boundary alignments are analyzed. The microband formation mechanism is analyzed in terms of the associated characteristic dislocation configurations.

* Corresponding author. Tel: +49 2116792 407; e-mail: i.gutierrez@mpie.de

1359-6462/$ - see front matter © 2013 Acta Materialia Inc. Published by Elsevier Ltd. All rights reserved.
http://dx.doi.org/10.1016/j.scriptamat.2013.03.010

The high-Mn steel used in this study had the chemical composition Fe–22Mn–0.6C (wt.%). Details on alloy processing can be found in Ref. [1]. The hot-rolled material showed a fully austenitic structure with an average grain size of 50 μm, which remained stable during deformation at room temperature. Tensile and shear tests were carried out at room temperature at an initial strain rate of 5×10^{-4} s^{-1} to an equivalent true strain of 0.1. At this strain level, the deformation structure mainly consists of dislocation substructures with few deformation twins [1]. The tensile bone-shaped samples had a gauge length of 8 mm, a gauge width of 2 mm and a gauge thickness of 1 mm. Shear deformation tests were performed using a shear test set-up described in Ref. [16]. The shear samples had a rectangular shape of dimensions $40 \times 14 \times 2$ mm^3. Dislocation substructures were investigated by combined ECCI and EBSD. Longitudinal sections of the tensile deformed sample, i.e. the section perpendicular to the tensile axis, were examined. In the sample deformed by shear, the shear direction (SD)–normal direction (ND) section was characterized. High-resolution EBSD maps (step size of 50–100 nm) were taken in a 6500 F JEOL field emission gun-scanning electron microscope equipped with a TSL OIM EBSD system. Dislocation substructures of the grains mapped by EBSD were subsequently examined by ECCI under controlled diffraction conditions, as described in previous works [1,3,4,17–19]. ECCI images were obtained with optimum contrast by tilting the matrix crystal into the Bragg condition to obtain high-intensity reflections and to excite the corresponding diffraction vector in a "two-beam" condition. ECCI observations were carried out in a Zeiss Crossbeam instrument (XB 1540, Carl Zeiss SMT AG, Germany) operated at 10 kV.

We examined the dislocation substructures in about 35 individual grains for both tensile- and shear-deformed specimens. Both samples were loaded with an initial strain rate of 5×10^{-4} s^{-1} to an equivalent true strain of 0.1. Substructure analysis was conducted by combined ECCI and EBSD. The experimentally analyzed crystal orientations in the sample deformed under tension are shown in the tensile axis inverse pole figure (TA-IPF) of Figure 1(a). The data provide a good representation of the deformation texture at 0.1 true strain [1]. The dislocation substructure is formed by two types of dislocation patterns, namely, cell blocks (CBs; Fig. 1(b)) and dislocation cells (DCs; Fig. 1(c)). The formation of these dislocation patterns is associated with the multiple character of slip, i.e. wavy and planar [3]. CB is the most common type of dislocation pattern. It is delimited by GNBs (highly-dense dislocation walls, HDDWs) and IDBs, which are also termed dislocation walls [7,8]. These dislocation configurations are imaged by ECCI as bright and compact layers (HDDWs) which are subdivided by finer bright layers (dislocation walls; Fig. 1(b)). CBs are formed in grains oriented along the line between the ⟨001⟩//TA and ⟨111⟩//TA crystallographic directions. Grains oriented close to ⟨112⟩//TA directions develop HDDWs that are parallel within 1°–2° to the {111} plane traces, i.e. they represent crystallographic boundaries. In contrast, grains close to the texture fiber comprising ⟨111⟩//TA directions build up non-crystallographic HDDWs which deviate up to 10° from the {111} slip planes. Equiaxed DCs are built up in grains oriented close to ⟨001⟩//TA directions (Fig. 1(c)). Dislocation substructures similar to those found here have been reported in medium-to-high stacking fault energy metals, such as copper and aluminum, deformed under tension [20,21]. Detailed examination of the dislocation boundaries, in particular of the HDDWs, did not reveal any effect of strain localization on the dislocation patterning such as microbanding.

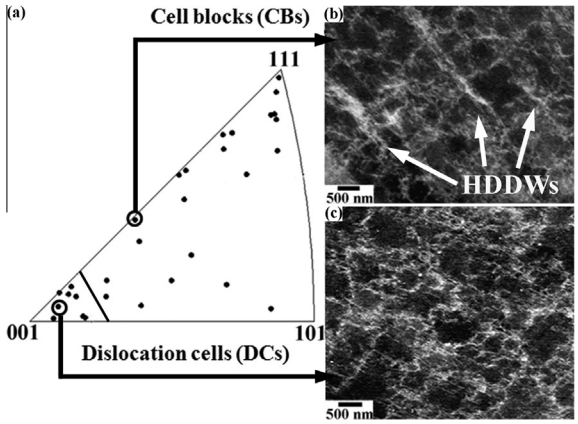

Figure 1. Crystallographic orientation dependence of the dislocation pattern in an Fe–22Mn–0.6C (wt.%) steel tensile deformed to 0.1 true strain. HDDWS: Highly-dense dislocation walls.

Figure 2(a) shows the SD-IPF containing the experimental crystal orientations of the analyzed grains in the sample deformed by shear. The crystals inspected also provide a good representation of the deformation texture at 0.1 equivalent true strain. At this strain level, the dislocation substructure mainly consists of CBs. DCs were observed in only a few grains. Analysis of the dislocation boundary alignment by combined ECCI and EBSD revealed that most of the HDDWs delimiting the CBs are non-crystallographic boundaries, which deviate by up to 10° from the {111} slip planes. Figure 2(b) shows an ECCI image of the CB structure developed in a grain oriented close to the ⟨213⟩//SD direction, where HDDWs are formed almost parallel to the {351} planes. The crystallographic plane trace analysis was carried out by using combined ECCI and EBSD mapping. Detailed examination of the CB structure by ECCI revealed that microbanding is strongly promoted in the sample deformed by shear when compared to the tensile deformed sample. Figure 3(a) shows a high-resolution EBSD map

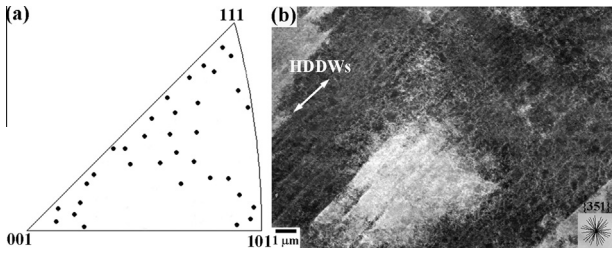

Figure 2. (a) IPF along the shear reference direction showing experimental grain orientations of a sample deformed by shear to 0.1 equivalent true strain. (b) ECCI image of the cell block structure developed in a grain oriented close to ⟨213⟩//SD direction. HDDWs are almost parallel to {351} planes (plane trace analysis was carried out by combined ECCI and EBSD).

of the CB structure developed in a grain oriented close to the ⟨1 0 1⟩//SD direction. The EBSD map displays the orientation gradients calculated with respect to the reference point in the map that contains the lowest kernel average misorientation value (blue–red: 0°–10°). The misorientation profile along several dislocation substructures (indicated by an arrow in Fig. 3(a)) is shown in Figure 3(b). This figure reveals that the CB structure developed in shear at 0.1 equivalent true strain is formed by low-angle dislocation boundaries with misorientations <2°. Detailed examination of the dislocation substructure by ECCI revealed that this structure is formed by cell blocks and microbands (indicated by arrows in Fig. 3(c)). Specifically, we observed lenticular-shaped microbands along the HDDWS of the existing CBs. These dislocation configurations are formed by pairs of dislocation layers spaced between 200 and 500 nm. The ECCI image in Figure 3(d) shows a detailed view of the internal dislocation structure of a microband. Under the current diffraction conditions, the crystal matrix appears dark and dislocations appear as sharp bright lines due to the electron channeling mechanism [17,22]. This figure reveals that the dislocation configuration is mainly formed by straight dislocations lying along the [1 0 1] crystallographic direction. The analysis of the dislocation reactions produced by the interaction between the active slip systems shows that these dislocations are Lomer–Cottrell dislocations. Following Schmid and Boas's labeling of face-centered cubic (fcc) slip systems [23], we obtain the following Schmid factors (SFs) for the slip systems of the crystal containing the microband shown in Figure 3(d) (only slip systems with SFs above 0.5 are considered): SF = 1.0 (D6), SF = 0.8 (B5), SF = 0.6 (B2 and C5). According to Thomson's tetrahedron [24], short-range interaction among dislocations pertaining to slip systems D6 and B2 results in the formation of Lomer–Cottrell locks. The formation of Lomer–Cottrell locks at microband interfaces has been considered recently in discrete dislocation dynamic simulations of the internal dislocation substructure of microbands in a Cu single crystal deformed by shear [25].

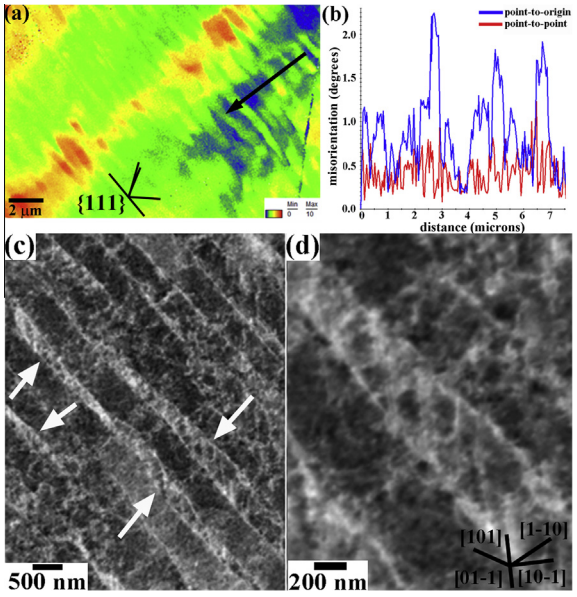

Figure 3. Cell block structure developed in a grain oriented close to the ⟨1 0 1⟩//SD direction of an Fe–22Mn–0.6C (wt.%) steel deformed by shear to 0.1 true strain. (a) Orientation gradients calculated with respect to the reference point in the map containing the lowest kernel average misorientation value (blue–red: 0°–10°). (b) Misorientation profile along several dislocation substructures (indicated by an arrow in (a)). (c) ECCI image of the dislocation substructure. Arrows indicate microbands. (d) ECCI image of the internal dislocation structure of a microband.

Comparison of the dislocation patterns formed under tension and shear reveals that in the Fe–22Mn–0.6C (wt.%) steel microbanding is strongly dependent on the strain path. This can be explained in terms of Schmid's law: shear deformation promotes slip concentration on single or coplanar slip. Stable crystal orientations under shear such as ⟨1 1 2⟩//SD and ⟨1 0 1⟩//SD have slip systems with Schmid factors near 1, resulting in enhanced shear localization. This result agrees with the intense microbanding activity observed in solid-solution fcc alloys such as Ni–Co and Al–Mg deformed by torsion or cold rolling [26,27]. In these studies, microbands similar to those studied here were observed. They were termed "first-generation microbands" [26,27]. However, the internal dislocation configuration of these first-generation microbands was not investigated. The current ECCI observations reveal that specific dislocation configurations inside microbands are created, namely, Lomer–Cottrell dislocations (Fig. 3(c)). These sessile dislocations play an important role in strain hardening due to the forest-type hardening associated with short-range dislocation interactions [24]. This hardening mechanism results in a higher critical stress when transferring plastic deformation across the microband. Accordingly, the overall stress can be written as the sum of two terms, namely, the stress required to transfer plasticity across a dislocation boundary with low misorientation, $\tau_{\text{transfer}} \sim Gb(\theta/Db)^{1/2}$ (where G is the shear modulus, b is the magnitude of Burgers vector, D is the microband size and θ is the misorientation angle) [28,29], and a Taylor term associated with short-range dislocation interactions within the microband interior, $\tau_{\text{Taylor}} \sim \alpha G b \rho^{1/2}$ (where α is the forest interaction parameter and ρ is the dislocation density). The first term can be also written in terms of the density of GNDs forming the microband boundary. This hardening term has recently been proposed as a relevant strain hardening mechanism in FeMnAlC alloys, the so-called microband-induced plasticity effect [10,15]. Further work is required to quantitatively evaluate the contribution of the hardening mechanism associated with microbanding to the strain hardening behavior of high-Mn steels.

There are two types of microbanding mechanisms proposed for fcc metals, namely, the double cross-slip model [30] and the dislocation boundary splitting mechanism [26,27]. In the first mechanism, microbanding is ascribed to unstable glide on latent slip systems involving pronounced dislocation cross-slip activity. This mechanism enables microbands to accommodate only modest lattice rotations; accordingly, their misorientation angles are small (misorientation angles below 1° are predicted) [30]. In the second mechanism, the driving force for microband nucleation is the high misorientation of the dislocation boundaries delimiting the existing

dislocation substructure [26,27]. As the misorientation of the dislocation walls forming the microbands is preserved during the boundary-splitting mechanism, the resulting microbands contain high misorientation angles, typically larger than 1°. Our observations reveal that microbanding in the present Fe–Mn–C alloy deformed by shear can be explained in terms of the dislocation boundary splitting mechanism. Microbands are nucleated at HDDWs, which provide the dislocation sources to build up the dislocation walls required in the microband formation process. They subsequently grow by a dislocation boundary-type splitting mechanism involving the activation of dislocation cross-slip. As most of the HDDWs delimiting the CB structure in the sample deformed by shear are non-crystallographic (they deviate by up to 10° from the {1 1 1} planes), this implies that microbands are non-crystallographic boundaries as well. We have recently reported the formation of crystallographic microbands in a tensile-deformed Fe–30.5Mn–2.1Al–1.2C (wt.%) steel [4]. In this alloy microbands were observed in grains oriented favorably to single or coplanar slip. They are characterized as paired dislocation sheets of about 100 nm thickness with low internal dislocation densities that remain as in-grain dislocation configurations. Microbands were not associated with any existing dislocation configuration. These observations indicate that microbanding in the Fe–Mn–Al-C alloy deformed under tension follows a double-cross slip mechanism. These findings reveal that both crystallographic and non-crystallographic microbands can be formed in high-Mn steels. This result may have a significant influence on the strain hardening behavior and plastic anisotropy of high-Mn steels. We would also like to point out the correlation found between the crystallographic character of the microbands and the microbanding mechanism. Further work is required to understand the influence of alloying and strain path effects on microbanding. In particular, we expect that the carbon content plays an important role in microbanding due to its strong influence on dislocation cross-slip in fcc metals [4,31]. For instance, we have recently addressed the role of carbon in dislocation patterning in an Fe–Mn–Al–C alloy [4]. As cross-slip is a stress-assisted mechanism, it results in a pronounced dependence of the dislocation pattern on the macroscopic resolved stress. However, as microbanding requires the activation of cross-slip on a shorter scale, its dependence on the carbon content is expected to be lower than that of dislocation patterning, where significant variations in cross-slip frequency are required to modify the patterns.

In summary, we have investigated the dislocation substructures, in particular those associated with microbands, obtained under different strain paths, namely, tension and shear, in an Fe–22Mn–0.6C (wt.%) high-Mn TWIP steel. Evaluation of the dislocation substructures by combined EBSD and ECCI mapping revealed that microbanding is dependent on the type of strain imposed. We explain this effect in terms of Schmid's law. We also observe that microbanding in the sample deformed by shear has a non-crystallographic character, which is associated with the existing cell block structure. Examination of the internal dislocation configuration of microbands provides new insights into the hardening mechanism associated with microbanding. Further work is, however, required to evaluate the contribution of this hardening mechanism to the overall strain hardening behavior of high-Mn steels.

The authors acknowledge the financial support by the German Research Foundation in the framework of the SFB 761 "steel ab initio". We would also like to thank Dr. J.A. del Valle (CENIM-CSIC) for performing the shear tests.

[1] I. Gutierrez-Urrutia, D. Raabe, Acta Mater. 59 (2011) 6449.
[2] I. Gutierrez-Urrutia, D. Raabe, Mater. Sci. Forum 702–703 (2012) 523.
[3] I. Gutierrez-Urrutia, D. Raabe, Scripta Mater. 66 (2012) 992.
[4] I. Gutierrez-Urrutia, D. Raabe, Acta Mater. 60 (2012) 5791.
[5] I. Gutierrez-Urrutia, D. Raabe, Scripta Mater. 68 (2013) 343.
[6] D.R. Steinmetz, T. Jäpel, B. Wietbrock, P. Eisenlohr, I. Gutierrez-Urrutia, A. Saeed-Akbari, T. Hickel, F. Roters, D. Raabe, Acta Mater. 61 (2013) 494.
[7] D.A. Hughes, N. Hansen, D.J. Bammann, Scripta Mater. 48 (2003) 147.
[8] N. Hansen, D.J. Jensen, Philos. Trans. R. Soc. 357 (1999) 1447.
[9] N. Hansen, Metall. Mater. Trans. A 32A (2001) 2917.
[10] J.D. Yoo, K.-T. Park, Mater. Sci. Eng. A 496 (2008) 417.
[11] J.D. Yoo, S.W. Hwang, K.-T. Park, Metall. Mater. Trans. A 40A (2009) 1520.
[12] K.-T. Park, G. Kim, S.K. Kim, S.W. Lee, S.W. Hwang, C.S. Lee, Metall. Mater. Int. 16 (2010) 1.
[13] K. Shen, B.J. Duggan, Acta Mater. 55 (2007) 1137.
[14] Q.Z. Chen, A.H.W. Ngan, B.J. Duggan, Proc. R. Soc. London A 459 (2003) 1661.
[15] K.-T. Park, Scripta Mater. 68 (2013) 375.
[16] I. Gutierrez-Urrutia, J.A. del Valle, S. Zaefferer, D. Raabe, J. Mater. Sci. 45 (2010) 6604.
[17] I. Gutierrez-Urrutia, S. Zaefferer, D. Raabe, Scripta Mater. 61 (2009) 737.
[18] I. Gutierrez-Urrutia, D. Raabe, Scripta Mater. 66 (2012) 343.
[19] A. Eisenlohr, I. Gutierrez-Urrutia, D. Raabe, Acta Mater. 60 (2012) 3994.
[20] G. Winther, Acta Mater. 56 (2008) 1919.
[21] X. Huang, G. Winther, Philos. Mag. 87 (2007) 5189.
[22] A.J. Wilkinson, P.B. Hirsch, Micron 28 (1997) 279.
[23] E. Schmid, W. Boas, Kristallplastizität mit besonderer Berücksichtigung der Metalle, Springer-Verlag, Berlin, 1935.
[24] J.P. Hirth, J. Lothe, Theory of Dislocations, McGraw-Hill, New York, 1982.
[25] O. Dmitrieva, J.V. Svirina, E. Demir, D. Raabe, Model. Simul. Mater. Sci. Eng. 18 (2010) 085011.
[26] D.A. Hughes, W.D. Nix, Mater. Sci. Eng. A 122 (1989) 153.
[27] D.A. Hughes, Acta Metall. Mater. 41 (1993) 1421.
[28] D.A. Hughes, N. Hansen, Acta Mater. 48 (2000) 2985.
[29] B. Liu, D. Raabe, P. Eisenlohr, F. Roters, A. Arsenlis, G. Hommes, Acta Mater. 59 (2011) 7125.
[30] P.J. Jackson, Scripta Metall. 17 (1983) 199.
[31] K. Sekido, T. Ohmura, L. Zhang, T. Hara, K. Tsuzaki, Mater. Sci. Eng. A 530 (2011) 396.